ChemCatChem

Research Article
doi.org/10.1002/cctc.202400655

Chemistry Europe
European Chemical Societies Publishing

www.chemcatchem.org

Mechanistic Insight into Alkali-Metal-Mediation of Styrene Transfer Hydrogenation: A DFT Study

Keelan M. Byrne,[a] Stuart D. Robertson,[c] Robert E. Mulvey,[c] and Tobias Krämer*[a, b]

A computational mechanistic study was performed to investigate the transfer hydrogenation of styrene catalysed by a potassium tris-hexamethyldisilazide magnesiate in the presence of 1,4-cyclohexadiene. Exploiting cooperative effects between Mg and K centres present in this tris(amide) complex results in the selective formation of the desired product ethylbenzene. The calculations demonstrate the synergy of the metal centres within the bimetallic complex, since neither the monometallic potassium amide K(HMDS) nor the magnesium amide Mg(HMDS)$_2$ on their own can efficiently execute this transformation under the experimental conditions. Several distinct mechanistic pathways have been explored, leading to the identification of the most plausible sequence in which both metal centres act in a synchronised manner.

Introduction

Catalytic hydrogenation of unsaturated bonds is a fundamental reaction in the Chemist's synthetic toolbox, finding utility in both industrial and laboratory settings.[1,2] Traditional catalytic systems such as those associated with the names of Wilkinson, Crabtree, and Noyori are based on late transition metals and commonly use molecular hydrogen as the reducing agent.[3,4] Overall these catalytic systems exhibit excellent performance under mild conditions along with high selectivity and functional group tolerance. However, with a view to generating greener and more sustainable strategies for catalysis in the future, substitution of the often scarce, expensive, and toxic precious transition metals with less problematic alternatives is a major goal in current research. Considering their low toxicity and relative abundance, and despite their limited redox chemistry, compounds of group 1 and 2 elements have become key targets as potential mediators in chemical transformations. Their utility in catalytic hydrogenations, usually in the form of highly reactive monometallic metal hydride complexes in which the electropositive s-block metal endows the hydride ligand with a strong nucleophilic character able to insert into unsaturated multiple bonds, is increasingly gaining recognition with several seminal papers published.[5–15] For example, Harder demonstrated alkene and imine hydrogenation with alkaline earth metal amides of the form Ae(HMDS)$_2$ [Ae = Mg, Ca, Sr, Ba; HMDS = 1,1,1,3,3,3-hexamethyldisilazide].[16,17] This process occurred at remarkably low H_2 pressure (p = 1–6 bar) and relatively low temperature (T = 80 °C). Whilst magnesium displayed no activity for alkene hydrogenation, conversion rates increased with metal size upon descending the group from calcium to barium. Various alkene substrates could be reduced, including activated (e.g. styrene), semi-activated (e.g. norbornadiene) or isolated non-activated (e.g. 1-hexene) C=C double bonds. Further improvement of activity and substrate scope was achieved by increasing the bulkiness of the amide ligands,[18] preventing formation of aggregates of higher nuclearity and hence increasing the concentration of catalytically active smaller metal hydride species. Theoretical studies on these systems have correlated the higher activation energies observed for the Mg-based catalyst to unfavourable linear bond angles in the active magnesium hydride intermediate (due to absence of d-orbital participation), the relatively high covalency of the magnesium hydride bond,[19] as well as charge and size of the metal ion.[20] The Harder group also demonstrated that the heavier alkaline earth bisamides can accomplish transfer hydrogenation of alkenes with 1,4-cyclohexadiene (1,4-CHD) acting as hydrogen source.[21] In this reaction, initial formation of the active catalyst species occurs through deprotonation of 1,4-CHD by Ae(HMDS)$_2$ (Ae = Ca, Sr, Ba) to form an unstable Meisenheimer intermediate, which subsequently undergoes β-hydrogen elimination to furnish the corresponding Ae–H hydride catalyst species concomitantly with benzene. As in the case of the alkene hydrogenation, magnesium also displayed no activity in this process.

In recent years examples of bimetallic cooperativity have emerged, in which an alkali metal enhances the catalytic propensity of another metal such as magnesium, calcium, zinc, aluminium or gallium.[22–24] Such alkali-metal-mediated (AMM) reactions often surpass the reactions of their monometallic counterparts in terms of reactivity and selectivity. Within these bimetallic partnerships the cooperative effect from the alkali metal can be due to (i) enhancement of the reactivity of the

[a] K. M. Byrne, Dr. T. Krämer
Department of Chemistry, Maynooth University, Maynooth, Co. Kildare, Ireland
E-mail: tobias.kraemer@mu.ie

[b] Dr. T. Krämer
Hamilton Institute, Maynooth University, Maynooth, Co. Kildare, Ireland

[c] Dr. S. D. Robertson, Prof. R. E. Mulvey
Department of Pure and Applied Chemistry, University of Strathclyde, Glasgow, G1 1XL, UK

Supporting information for this article is available on the WWW under https://doi.org/10.1002/cctc.202400655

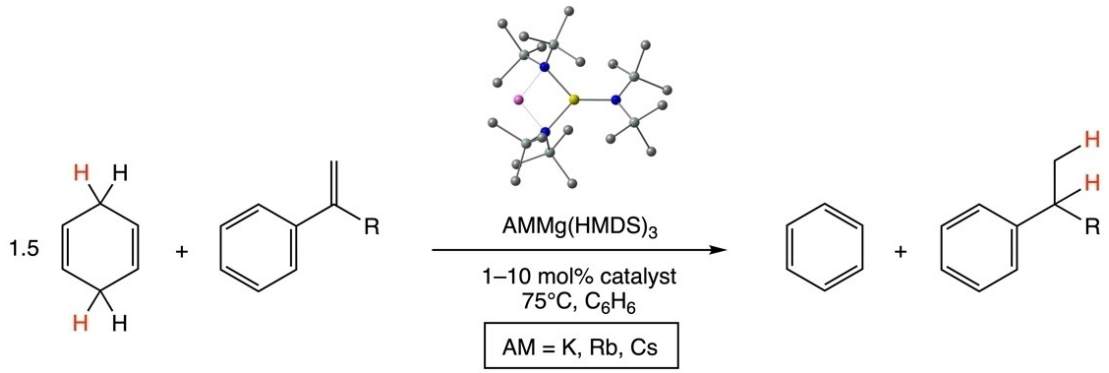

Figure 1. Transfer hydrogenation catalysis by $AMMg(HMDS)_3$ in the presence of 1.5 equivalents of 1,4-cyclohexadiene as hydrogen source and substrates styrene (R = H) and 1,1-diphenylethene (R = Ph).

nucleophile, (ii) activation of the substrate by polarisation of its unsaturated bonds, (iii) enhancement of the Lewis acidity at the catalytic centre and (iv) anchoring the substrate in proximity to the catalytic centre. This effect is for example evident in the lithium-aluminate catalysed hydroboration of aldehydes, ketones and imines, where a key hydrido aluminate intermediate is more polarised in the bimetallic compound relative to its neutral counterpart which displays higher reactivity.[25] In a related system, lithium helps to increase the Lewis acidity of the reactive aluminium centre, facilitating hydrophosphination of a range of unsaturated bonds.[26] In the hydroamination of alkenes and alkynes catalysed by bimetallic alkali metal magnesiates, the alkali metal cation enhances the susceptibility of the unsaturated substrate towards nucleophilic attack by the amide anion.[27] Following the first report by Harder on heterobimetallic hydrogenation catalysis with $LiAlH_4$,[12] the Guan group has explored similar synergistic effects to catalyse hydrogenation of styrene and α-alkenes with heterobimetallic s-block metal hydrides by combining KH and alkaline earth metal amides $Ae(HMDS)_2$ (Ae = Mg, Ca).[28] The bimetallic catalyst exhibited superior activity than its components on their own, although the active species itself could not be authenticated. It was hypothesised that in case of Ae = Mg the ate complex $[K(HMDS)_2MgH]_2$ is a likely candidate. Exploiting AMM in a similar attempt to activate $Mg(HMDS)_2$ for transfer hydrogenation of alkenes, Mulvey and co-workers systematically explored the effect of an added alkali metal on the transfer hydrogenation of the benchmark alkenes styrene and 1,1-diphenylethene (DPE). This group utilized defined heterobimetallic complexes of the form $AMMg(HMDS)_3$, where AM is an alkali metal, in the presence of 1,4-CHD (Figure 1).[29]

Screening of the alkali metals revealed the most efficient synergistic partnerships exerted on the magnesium centre by the alkali metal. The general increase in reactivity followed previously reported trends, that is, descending down the group (Li–Cs) gave increased reaction rates, albeit at a modest expense of selectivity (onset of polymerisation). For the substrate styrene and a catalyst loading of 10%, conversion in excess of 98% was achieved after 3.5, 0.75 and 0.5 hours for $KMg(HMDS)_3$, $RbMg(HMDS)_3$ and $CsMg(HMDS)_3$, respectively. The monometallic counterparts $Mg(HMDS)_2$ and K(HMDS), on their own effected little or no catalytic activity (or activity with loss of selectivity). Thus, this unequivocally demonstrated the synergistic effect of these bimetallic partnerships and provided proof-of-concept that the performance of even the most unreactive Ae metal could be effectively boosted when paired with the correct alkali metal. Based on combined experimental and computational mechanistic insight derived from Harder's transfer hydrogenation with $Ca(HMDS)_2$, a plausible catalytic pathway proceeding via a hydride magnesiate complex was proposed (Figure 2).

The tris-HMDS complex deprotonates 1,4-CHD under liberation of HMDS(H) and formation of an unstable Meisenheimer complex, which immediately undergoes β-hydrogen elimination to form the catalytically active mixed-metal hydride compound and benzene. The hydride complex then undergoes insertion into the double bond of styrene to form an intermediate heterobimetallic alkyl complex, which upon protonation by the previously released HMDS(H) forms ethylbenzene as the desired product and regenerates the catalyst.

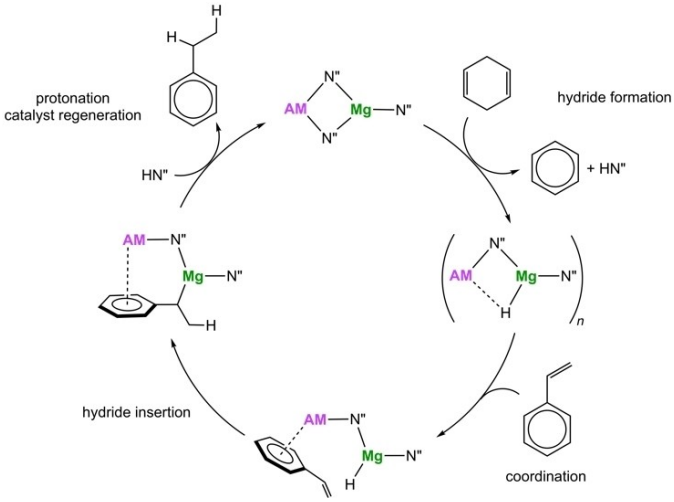

Figure 2. Proposed reaction mechanism for transfer hydrogenation of styrene with 1,4-CHD catalysed by $AMMgN''_3$ [AM = alkali metal, N'' = N-$(SiMe_3)_2$].

Despite the generally accepted mechanistic picture for these type of systems, detailed computational studies on the specific effects of the alkali metal in promoting the reactivity of another metal in the mechanism of heterobimetallic s-block metal catalysis are rather scarce.[30] However, such insight at the atomic structure level is critical for a systematic design of improved catalyst platforms. The tendency of alkali metal magnesiates to form clusters of higher nuclearity but often undefined aggregation state is well documented.[31] In the present system, several dimeric hydride magnesiates of the form $[AMMg(HMDS)_2H]_2$, which are proposed intermediates in the catalytic cycle, have been isolated and structurally characterised. Nonetheless, it is reasonable to study their reactivity with monomeric model systems in order to gain insight into the individual roles of their constituent units (K^+, Mg^{2+} and HMDS) in the reaction mechanism. As has been argued elsewhere, under catalytic turnover conditions the initial concentration of the monomeric catalyst precursor from which the hydride catalyst species are formed from reaction with 1,4-CHD is very low (1–10 mol%).[19] To form dimeric aggregates these monomers will need to encounter each other through diffusion, but encounters with the excess substrate are going to occur with a higher probability. Thus, we have used quantum chemical calculations to elucidate possible mechanistic pathways for transfer hydrogenation of the benchmark substrate styrene, as well as potential side reactions, mediated by Mulvey's $KMg(HMDS)_3$ complex. In comparing the performance of the bimetallic catalyst in this transfer hydrogenation to that of the isolated $Mg(HMDS)_2$ and K(HMDS) species on their own, we aim to delineate the cooperative role of the two metal centres in the combined system.

Results and Discussion

First we explored the reactivity of the magnesium bisamide, $Mg(HMDS)_2$ in the absence of alkali metal mediation. The Free Energy profile associated with this reaction obtained at the PBE-D3(BJ)/def2-QZVP//TPSS-D3(BJ)/def2-TZVP/def2-SV(P) level of theory is depicted in Figure 3. All Gibbs Free Energies (ΔG_{348}) are reported at $T = 75\,^{\circ}C$ and are corrected for effects from benzene solvent.

Formation of the active magnesium hydride species is initiated by binding of 1,4-CHD to the linear $Mg(HMDS)_2$ complex (MgN''_2, $N'' = HMDS$) and its subsequent deprotonation via **Mg-TS1**. This step has a substantial energetic barrier of 32.1 kcal mol^{-1}, and results in an unstable Meisenheimer complex (**Mg-I2**) at 19.5 kcal mol^{-1}. Loss of disilazane N''H then enables hydride transfer from the cyclohexadienyl anion to the Mg centre via transition state **Mg-TS2** with a barrier of $\Delta G^{\ddagger} =$ 27.1 kcal mol^{-1}, somewhat lower than **Mg-TS1**. Following release of benzene from intermediate **Mg-I4**, formation of the active N''MgH catalyst (**Mg-cat**) is slightly endergonic ($\Delta G =$ 1.8 kcal mol^{-1}). Binding of styrene to N''MgH forming **Mg-I5** is also endergonic ($\Delta G = 7.1$ kcal mol^{-1}), and subsequent hydrogenation of the substrate commences with hydride transfer onto the terminal carbon of the ethenyl moiety. Transition state **Mg-TS3** connects **Mg-I5** to the alkyl intermediate **Mg-I6** via an energetic barrier of 19.2 kcal mol^{-1}. Formation of the benzyl magnesium species (**Mg-I6**) is moderately exergonic (−8.3 kcal mol^{-1}) and from here, ethylbenzene can be extruded as the final product by protonation with N''H via **Mg-TS4** ($\Delta G^{\ddagger} = 5.0$ kcal mol^{-1}) following prior coordination of the disilazane to the metal centre. The overall energy release for the transfer hydrogenation of styrene (1,4-CHD + styrene→benzene + ethylbenzene) is 34.4 kcal mol^{-1}, which is considerably more exergonic than hydrogenation by H_2 (cf. $\Delta G = -20.9$ kcal mol^{-1}) owing to the additional aromatization energy for conversion of

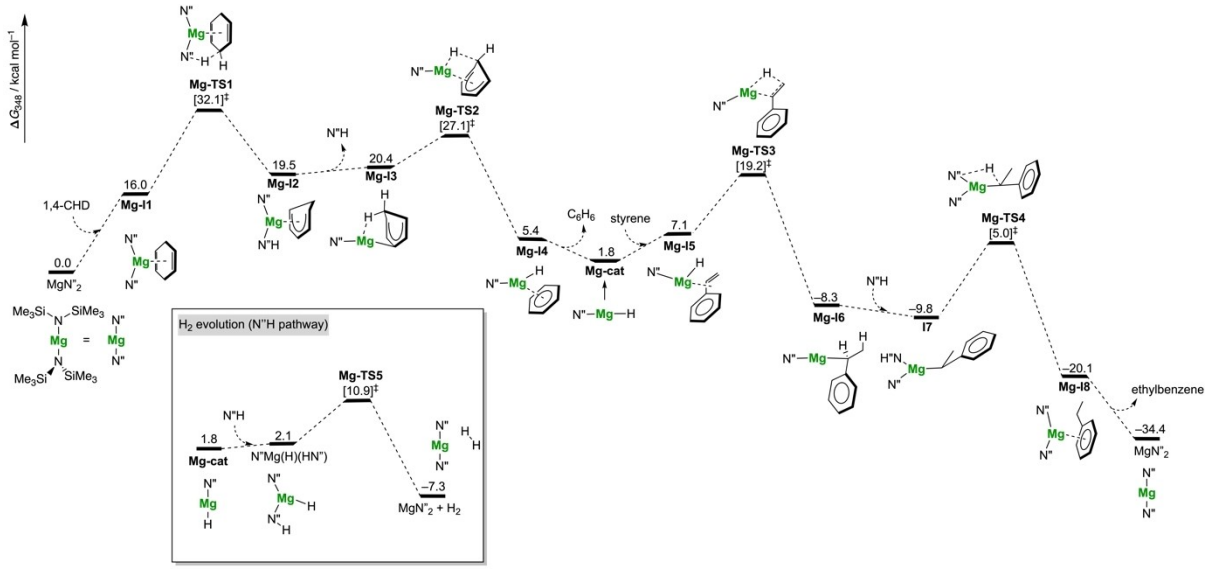

Figure 3. DFT-calculated Free Energy reaction profile (ΔG, T = 348.15 K, 1 mol L^{-1}) for transfer hydrogenation of styrene with 1,4-CHD and MgN''_2 [$N'' = N(SiMe_3)_2$].

1,4-CHD into benzene and H_2. It is noteworthy that evolution of H_2 via interception of **Mg-cat** by N″H represents a more favourable reaction, with an overall barrier of only 10.9 kcal mol^{-1}. The steps along the above pathway closely resemble those for the heavier Ca(HMDS)$_2$ homologue, with geometries of all stationary points being structurally similar to those reported by Harder (see Figure 4 for geometries of key transition states).[21]

Recalculation of the energetic profile for Ca(HMDS)$_2$ at the present level of theory gave close agreement with previously reported results (see Figures S1 and S2), and allowed for a direct comparison to Mg(HMDS)$_2$. For the magnesium congener the activation energy associated with the initial rate determining step (**TS1**) for deprotonation of 1,4-CHD is 11.7 kcal mol^{-1} higher in energy than for Ca(HMDS)$_2$, which is consistent with the absence of any catalytic reactivity for Mg(HMDS)$_2$ even at elevated temperatures (no conversion observed after 16 hours at 75 °C). Likewise, the hydride transfer step requires appreciably more activation energy for the Mg-based ($\Delta G^{\ddagger} =$ 17.4 kcal mol^{-1}, relative to **Mg-cat**) than for the Ca-based catalyst ($\Delta G^{\ddagger} = 7.0$ kcal mol^{-1}). This trend can be correlated to the decrease in Ae–H bond strength upon descending the group, as well as more favourable deformation energies associated with the changes in bond angles.[19] The optimised geometry of the MgH species has an N–Mg–H angle of 180°, which decreases to 134° for the CaH catalyst due to admixture of 3d orbital character into the Ca–H σ-bond. The same factors likely contribute to the higher activation energies for the final protonation step of the styryl intermediate **I6** through **TS4**, which differ by about 11 kcal mol^{-1} between Ca(HMDS)$_2$ and Mg(HMDS)$_2$, and the higher energetic penalty associated with substrate binding to the Mg(HMDS)$_2$ complex. Moreover, structural differences are observed for the intermediates and transition states along the sequence of hydrogen transfer steps. Whilst the Ca^{2+} ion is oriented more towards the phenyl ring of the styryl anion and stabilises the delocalised negative charge through cation π-interactions, the smaller (and harder) Mg^{2+} ion preferentially interacts strongly with the α-carbon centre (with no delocalisation of charge onto the ring system). This is similar to the relationship between benzyl anions and the neighbouring group 1 cations which show increasing M–Ph π -interactions on descending the group.[32]

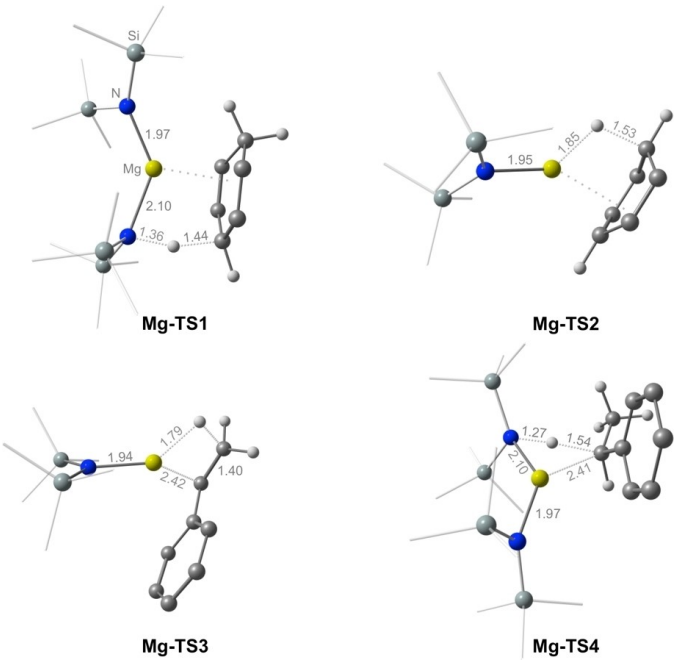

Figure 4. DFT-optimised geometries of all transition states along the pathway for transfer hydrogenation of styrene with 1,4-CHD and MgN″$_2$ showing key bond distances.

Next, we turned to the above reaction mediated by K(HMDS), the energy profile being shown in Figure 5. Based on structural data reported in the literature, the catalyst was modelled as a homometallic cyclodimer.[33] An alternative pathway involving the monomeric catalyst species was also calculated (see Figures S3 and S4), which serves as an additional point of reference for the discussion of the bimetallic catalyst system. The structure of dimeric [(C$_6$H$_6$)KN″]$_2$ displays two amide anions bridging the potassium ions and in addition, each K^+ ion is η^6-coordinated by one benzene molecule (see Figure S5). From inspection of the energy profile, it is immediately clear that individual steps along the reaction sequence are kinetically more favourable than in the case of monometallic Mg(HMDS)$_2$. Starting from the dimer, formation of the Meisenheimer intermediate **K-I2** is facile with an initial barrier to deprotonation of only 20.8 kcal mol^{-1} (**K-TS1**). The release of N″H furnishes isomer **K-I3** accompanied by structural rearrangement of the cyclohexadienyl carbanion coordination mode into a bridging position between both K^+ ions. Subsequent hydride transfer from the cyclohexadienyl unit occurs via **K-TS2** ($\Delta G^{\ddagger} =$ 24.3 kcal mol^{-1}) with a small activation energy of 12.3 kcal mol^{-1} relative to **K-I3**, forming the μ_2-bridged hydride intermediate **K-I4**. In the following styrene insertion the substrate coordinates in an η^6-fashion to one the K^+ ions, following displacement of benzene. Transfer hydrogenation proceeds via initial hydride transfer through transition state **K-TS3** with a relative energy barrier of 6.4 kcal mol^{-1}, leading to the complex **K-I6**. Protonation occurs through re-coordination of N″H and subsequent N–H activation via **K-TS4** and an associated relative barrier of 7 kcal mol^{-1}. Release of the alkyl product from **K-I8** completes the catalytic cycle and regenerates the catalyst. Apart from inserting into the styrene double bond, the *in situ* generated hydride intermediate is susceptible to undergoing two possible side reactions that compete with the desired product formation. Protonation of (C$_6$H$_6$)K(μ_2-H)(μ_2-N″)K(C$_6$H$_6$) (**K-I4**) by the initially formed N″H proceeds through transition state **K-TS5** ($\Delta G^{\ddagger} =$ 5.7 kcal mol^{-1}), thereby generating dihydrogen and reforming the catalyst [(C$_6$H$_6$)KN″]$_2$. Dihydrogen formation may also occur through the alternative deprotonation of 1,4-CHD via **K-TS6** with an associated barrier of $\Delta G^{\ddagger} = 14.4$ kcal mol^{-1}, although the activation energy is somewhat higher than those for the other processes. The observation of two competitive pathways for styrene reduction and dihydrogen evolution is in agreement with the experimentally observed immediate formation of dihydrogen gas along with consumption of the majority of 1,4-CHD with only 36% conversion of styrene after 3 hours at 75 °C.

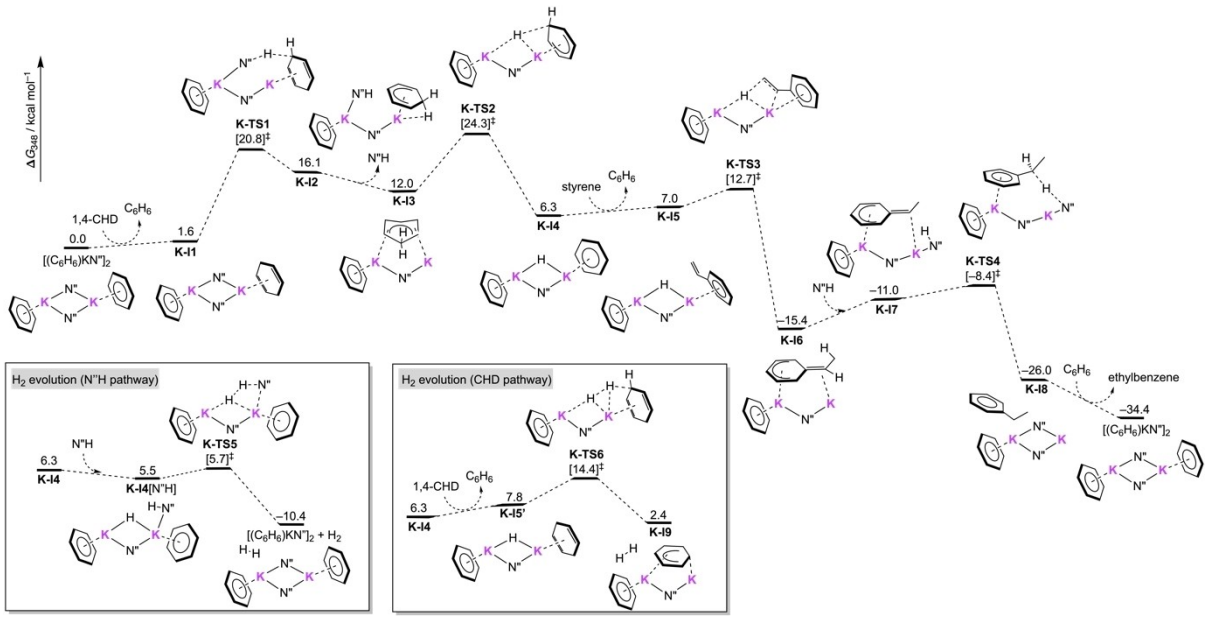

Figure 5. DFT-calculated Free Energy (ΔG, T = 348.15 K, 1 mol L^{-1}) reaction profile for transfer hydrogenation of styrene with 1,4-CHD and dimeric $[(C_6H_6)KN''_2]_2$.

The above results serve as a reference point for our further discussion, confirming that the two sole monometallic compounds are not competent catalysts in the transfer hydrogenation of styrene due to being either too unreactive or unselective. Next we turned to the analysis of the reaction mediated by the bimetallic catalyst.

The energy profile for formation of the magnesium hydride catalyst co-complexed by K(HMDS) is shown in Figure 6. Optimised geometries of key intermediates and transition states are depicted in Figure 7. In the initial step the hydrogen source, 1,4-CHD, replaces benzene and coordinates to the potassium ion in **R**, giving **I1** in a slightly exergonic process (ΔG = −2.5 kcal mol^{-1}). We envisioned that direct deprotonation of 1,4-CHD by one of the HMDS groups of the MgN''$_3$ unit could occur at this stage. However, the lowest transition state located for this process has a high activation barrier ($\Delta G^{\neq}$ =

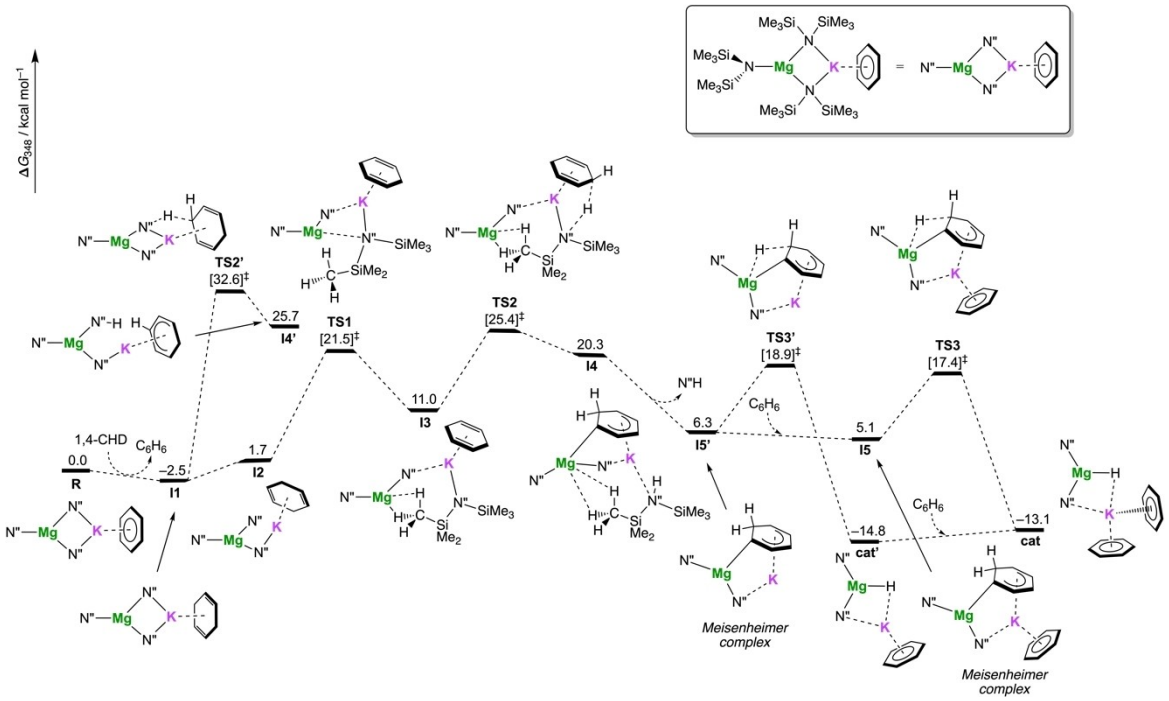

Figure 6. DFT-calculated Free Energy reaction profile (ΔG, T = 348.15 K, 1 mol L^{-1}) for the formation of the magnesium hydride catalyst from 1,4-CHD and $(C_6H_6)KMgN''_3$.

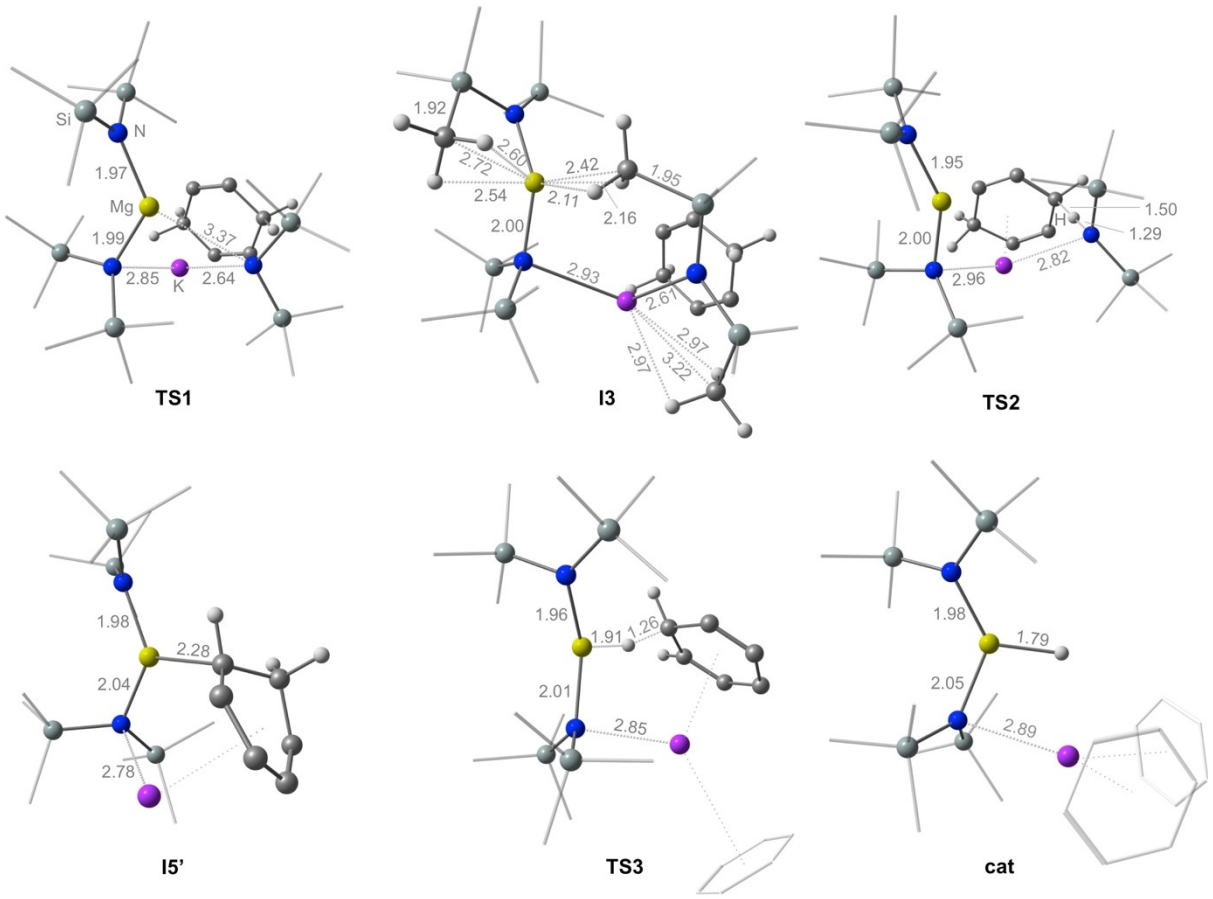

Figure 7. DFT-optimised geometries of key stationary points along the pathway for formation of magnesium hydride catalyst $(C_6H_6)_2KMg(H)N''_2$ showing key bond distances.

32.6 kcal mol^{-1}) which renders this step unviable under the experimental reaction conditions. An alternative pathway is enabled following dissociation of one of the bridging Mg-amide bonds via **TS1** ($\Delta G^{\ddagger} = 21.5$ kcal mol^{-1}) to furnish **I3** at an energy of 11.0 kcal mol^{-1}. In this intermediate the two metal centres are only connected by one N″ unit, whilst the other amide is terminally bound to the potassium ion. Both metals engage in intramolecular $CH_3\cdots K^+$ and $CH_3\cdots Mg^{2+}$ interactions featuring κ^2H contacts with the $N(SiMe_3)_2$ substituent.[34,35] The methyl group of the decoordinated HMDS nearest to the Mg ion is tilted towards this centre, borne out in the closing of the N–Si–C_β angle (105°) as compared to about 117° of the other two angles in this $Si(CH_3)_3$ unit. The Mg···C (2.42 Å) and corresponding Mg···H (2.11–2.16 Å) contacts of the tilted methyl group are short compared to the sum of their van der Waals radii. The N–C_β bond is longer by 0.04 Å than the other N–C_β bonds of the non-interacting "terminal" methyl groups. These structural parameters are reminiscent of the di-*tert*-butylmagnesium dimer and can be associated with agostic interactions.[36,37] An intramolecular agostic interaction can also be identified for one of the methyl groups of the coordinated HMDS ligands. Likewise, two hydrogens of a second methyl group on the decoordinated HMDS ligand are oriented towards the K^+ ion in an agostic-type fashion.[38] Together these secondary intramolecular interactions play a substantial role in the stabilisation of this molecular assembly. The increased basicity of the terminal (to K^+) amide and its favourable position relative to 1,4-CHD now enables its deprotonation. The deprotonation step proceeds via **TS2** with an overall energetic barrier at $\Delta G^{\ddagger} =$ 25.4 kcal mol^{-1}, substantially stabilised by about 7 kcal mol^{-1} relative to the direct deprotonation pathway. This eventually affords the Meisenheimer intermediate **I5′** at 6.3 kcal mol^{-1} following release of protonated N″H from intermediate **I4**.[39] The immediate barrier with respect to the preceding minimum **I3** amounts to only 14.4 kcal mol^{-1}, which is comparable to that calculated for the monomeric and dimeric K(HMDS) pathways. Despite the pre-alignment between K^+, 1,4-CHD and N″ in **I3** there is no obvious activation of the (H)C–H bond in 1,4-CHD ($r_{CH} = 1.10$ Å). A similar reaction sequence involving a preorganisation step of the catalyst to an "open form" was recently invoked in the mechanism for ferration of aromatic substrates by a bimetallic [(toluene)NaFe(HMDS)$_3$] complex in another example of AMM.[40]

Subsequent hydride elimination from the cyclohexadienyl anion by the MgN''_2 fragment can occur via **TS3** ($\Delta G^{\ddagger} =$ 17.4 kcal mol^{-1}) after complexation of the K^+ ion by benzene solvent, however, direct hydride transfer via **TS3′** ($\Delta G^{\ddagger} =$ 18.9 kcal mol^{-1}) in the absence of coordinated benzene is

competitive. This final step results in formation of $(C_6H_6)_2KMg(H)(HMDS)_2$ (**cat**), which can be considered in equilibrium with the benzene partially de-coordinated form $(C_6H_6)KMg(H)(HMDS)_2$ (**cat'**). It should be stressed that one benzene molecule has its origin in conversion of the unconjugated 1,4-CHD, whilst the second benzene stems from the solvent.

Thus, the calculations reveal that both metals play specific but equally important roles in promoting initial formation of the catalyst. In particular, potassium has a central role in facilitating deprotonation of 1,4-CHD, whereas the magnesium ion is central to stabilising the hydride catalyst.[41] The K^+ ion acts in two ways: firstly, it serves as a coordination site for 1,4-CHD, and secondly, it facilitates decoordination of one HMDS and ultimately deprotonation of 1,4-CHD. Both metal ions also act together in stabilising the negatively charged Meisenheimer intermediate. In comparison, this pathway has a lower overall activation energy span ($\Delta G^{\ddagger} = 27.9$ kcal mol^{-1} relative to **I1**) than the direct deprotonation route ($\Delta G^{\ddagger} = 35.1$ kcal mol^{-1}) and also more favoured than the deprotonation step in the pathway involving MgN''_2 in isolation ($\Delta G^{\ddagger} = 32.1$ kcal mol^{-1}). The initial deprotonation of 1,4-CHD also corresponds to the rate-determining step of the overall cycle, since it has the highest overall energy span ($\Delta G^{\ddagger} = 27.9$ kcal mol^{-1}) along the entire pathway, with those related to the transfer of hydride and proton onto styrene being much lower (see discussion below). This energetic barrier is consistent with an observed reaction time of approximately 3.5 hours at 75 °C.

We have probed the possibility that the transition state for proton abstraction from 1,4-CHD may be stabilised by cation π-interactions involving a second equivalent of $(C_6H_6)KMg(HMDS)_3$ (**R**). Recent DFT calculations have demonstrated the beneficial effect of such interactions in the nucleophilic alkylation of benzene by a Ca β-diketiminate complex.[42] However, in the present system, the barrier to deprotonation is only insubstantially affected in the bimetallic mechanism and its magnitude remains comparable to the most favoured monomeric pathway (see Figure S6). This implies that such reactions are only accelerated by π-arene···Ae metal contacts and require accessible (empty) d-orbitals on the metal centre (which is the case for Ca^{2+} but not for K^+). Based on these calculations the possibility of assembly of a transient inverse sandwich cannot be ruled out, however, onward reactivity would proceed in an analogous fashion to the mechanism established above. We further note in passing that any attempts to find pathways featuring initial coordination of 1,4-CHD to the Mg centre or hydride abstraction by the K^+ ion via a $(CHD^+)K–H$ intermediate were unsuccessful. The energy profile for the subsequent hydrogenation pathway is shown in Figure 8, starting from the bis-benzene catalyst species $(C_6H_6)_2KMg(H)(HMDS)_2$ (**cat**).

Following ligand exchange of one benzene, styrene binds to the K^+ ion in an η^4-fashion between the exocyclic double bond as well as the *ipso*- and *ortho*-carbon, forming **I6**. This intermediate could also be obtained from styrene coordination to **cat'** without notably affecting the following reactions energetically. Hydride transfer onto the β-carbon is facile and proceeds with a relative barrier of only 10.0 kcal mol^{-1} via **TS4**, leading to formation of the α-styryl magnesium intermediate α-**I7** at an energy of −24.9 kcal mol^{-1} (see Figure 9). In **TS4** the K^+ centre once more assumes its cooperative role through anchoring the styrene substrate and polarisation of its double bond, priming it for hydride transfer. The cooperative effect of both metals renders the activation energy of this step much lower than for isolated $Mg(HMDS)_2$, for which the barrier is 17.4 kcal mol^{-1}.

The optimised geometry of α-**I7** reveals that the structure is stabilised by a short Mg–C bond (2.22 Å) and a η^6-interaction between K^+ and the phenyl ring with a $K\cdots C_{centroid}$ separation of 3.08 Å. This bonding motif bears close resemblance to that in the experimental bimetallic complex $^tBu_2Zn(PhCH_2)K\cdot Me_6TREN$ [Me_6TREN = *tris*(*N*,*N*-dimethyl-2-aminoethyl)amine], in which the benzyl anion acts as a dual σ- and π-coordinating ligand (to Zn^{2+} and K^+, respectively).[43] The negative charge is dominantly located on the sp^3-hybridized C_α centre, as evidenced from inspection of the Mulliken charges.

Further, the C_α–C_{ipso} distance indicates the presence of a single bond, consistent with no delocalisation of the negative charge onto the ring. The magnesium centre adopts a distorted trigonal planar geometry surrounded by two nitrogen atoms of HMDS and the styryl $C(H)CH_3$ group. The next step involves quenching of the α-**I7** intermediate with N''H, which involves protonation of the strong Mg–C bond. After considering various

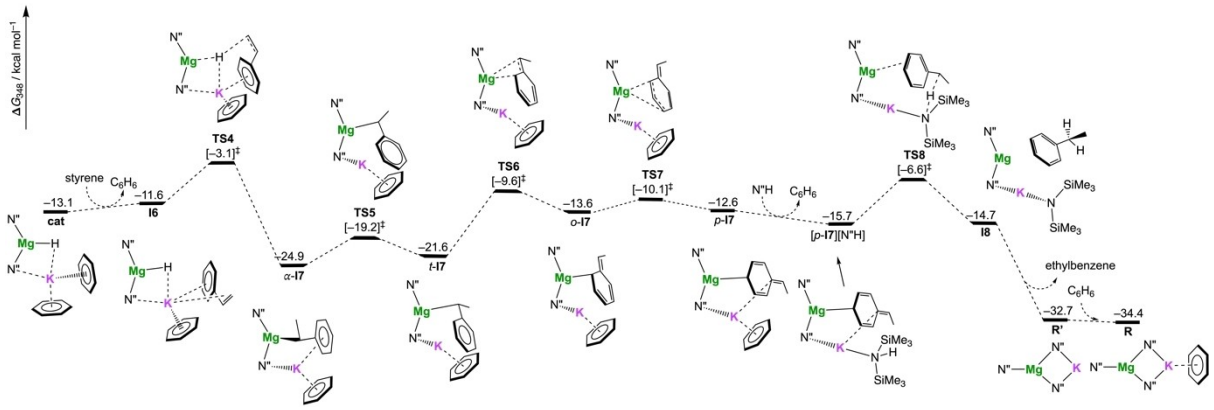

Figure 8. DFT-calculated Free Energy reaction profile (ΔG, T = 348.15 K, 1 mol L^{-1}) for styrene transfer hydrogenation by $(C_6H_6)_2K(H)MgN''_2$.

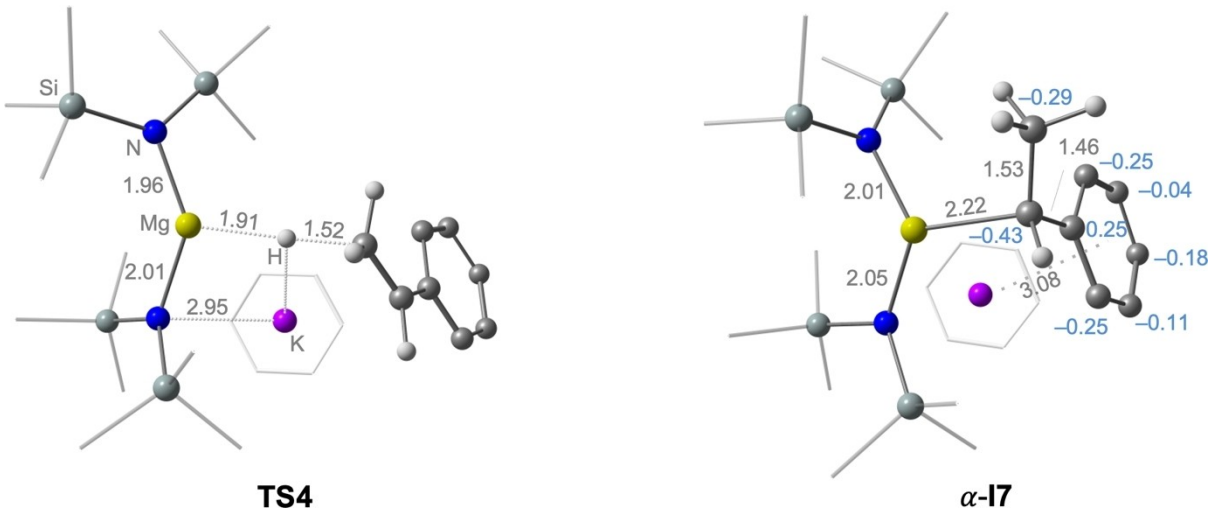

Figure 9. DFT-optimised geometries of the transition state **TS4** for hydride transfer forming the alkyl intermediate ***α*-I7** showing key bond distances and Mulliken charges (blue).

structures with and without the presence of benzene coordinated to the K^+ centre (see Supporting Information for details), it emerged that protonation necessitates decoordination of the C_α centre from Mg^{2+}. Using this rationale of initially disrupting the Mg^{2+}–C_α linkage, the most favourable pathway that achieves this involves a delocalisation of the negative charge from C_α to the *para*-position of the phenyl ring. Structures of all relevant stationary points along this pathway are shown in Figure 10. Initial rotation of the styryl moiety around the Mg^{2+}–C_α vector gives *t*-**I7** at -21.6 kcal mol^{-1} via the low-lying transition state **TS5** ($\Delta G^{\ddagger} = 5.7$ kcal mol^{-1}). It is apparent that stabilisation due to the face-on η^6-K^+···phenyl coordination amounts to about 3 kcal mol^{-1}. The following sequence of steps occurs with moderate barriers over **TS6** and **TS7** (approx. 15 kcal mol^{-1} relative to α-**I7**), ultimately leading to a stabilisation of the anionic carbon centre through shift of the coordination mode from C_α to the *para*-carbon of phenyl. In *p*-**I7** the negative charge is now delocalised onto the *para*-position of the ring with concomitant formation of an exocyclic C=C double bond and stabilised by the Mg^{2+} ion, while the K^+ ion interacts in an η^6-fashion with the planarised C=C(CH_3) unit. The intermediate structure *o*-**I7**, featuring a bond between Mg^{2+} and the *ortho*-C position, is found at -13.6 kcal mol^{-1}. Displacement of benzene by N″H and subsequent K^+ binding forms [*p*-**I7**][N″H] which is stabilised by 3.1 kcal mol^{-1} relative to *p*-**I7**. This complex is able to efficiently protonate the styryl moiety via **TS8** with an overall activation energy relative to α-**I7** of $\Delta G^{\ddagger} = 18.3$ kcal mol^{-1}. The resulting complex reforms the starting complex **R** in a barrierless process during geometry optimisation following removal of ethylbenzene and addition of one equivalent of benzene. Structures of optimised geometries are shown in Figure 11.

Several alternative pathways encompassing a proton shuttle, direct protonation at C_α, and initial coordination of N″H to Mg prior to proton transfer were found to be significantly higher in energy (see Supplementary Information for discussion). Noteworthy is the direct protonation of α-**I7**, the lowest pathway for this process occurring with an appreciable energetic barrier of 40.0 kcal mol^{-1}. Here N″H approaches the Mg–C_α bond in an S_N2-type trajectory, and proton transfer occurs with inversion at the C_α centre (Figure S7).

Two previously reported alternative pathways to product formation were also considered in the present context (Figure 12).[44] In the first of these, α-**I7** complexes with 1,4-CHD (displacing benzene and acting as a surrogate for N″H) to form **I9** and subsequently transfers a proton from 1,4-CHD to the substrate via **TS9**. The associated relative barrier for this step ($\Delta G^{\ddagger} = 31.9$ kcal mol^{-1}) is not competitive with the much more favourable proton transfer from N″H, and can be safely ruled out. The second of the alternatives shunts formation of the metal hydride catalyst altogether, and proceeds by styrene coordination to the Meisenheimer intermediate **I5′**. However, transfer of a hydride directly from the cyclohexadienyl anion to styrene comes with a more substantial barrier (**TS10**, $\Delta G^{\ddagger} =$ 31.7 kcal mol^{-1}) and is hence also unfeasible.

The computed pathways for potential side reactions are shown in Figure 13. Hydrogen formation can occur when N″H intercepts the hydride magnesiate catalyst. The overall barrier to this process via **TS11** is 21.2 kcal mol^{-1} and comparable to – but higher than – the overall barrier to protonation of α-**I7**. This result is consistent with experiment, where formation of small amounts of H_2 is observed. In contrast, the activation barrier to styrene polymerisation (**TS12**, $\Delta G^{\ddagger} = 31.6$ kcal mol^{-1}) is substantially higher than that of the hydrogenation pathway, and hence highly disfavoured for this system. This process would in principle only be observable in the absence of N″H.

During the experimental reduction of styrene with $NaMg(HMDS)_3$ precipitation of crystalline [{$NaMg(HMDS)_2H$}$_2$] was observed, however, formation of crystalline [$AMMg(HMDS)_2H]_2$ (AM = K, Rb, Cs) under the same conditions was not reported. The sodium species was also separately synthesised along with its potassium and rubidium analogues.

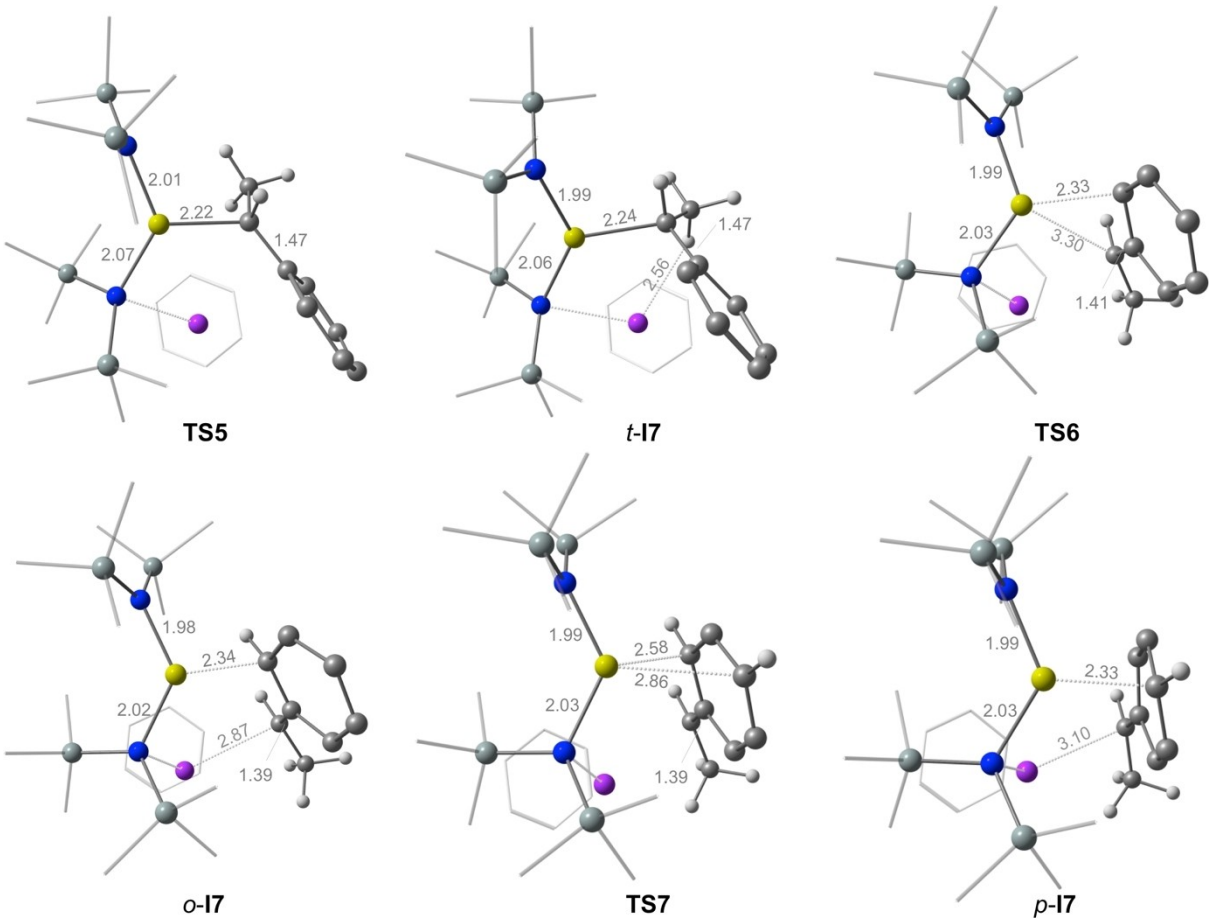

Figure 10. DFT-optimised geometries of the stationary points along the pathway for rearrangement of the alkyl intermediate α-**I7** to *p*-**I7** showing key bond distances.

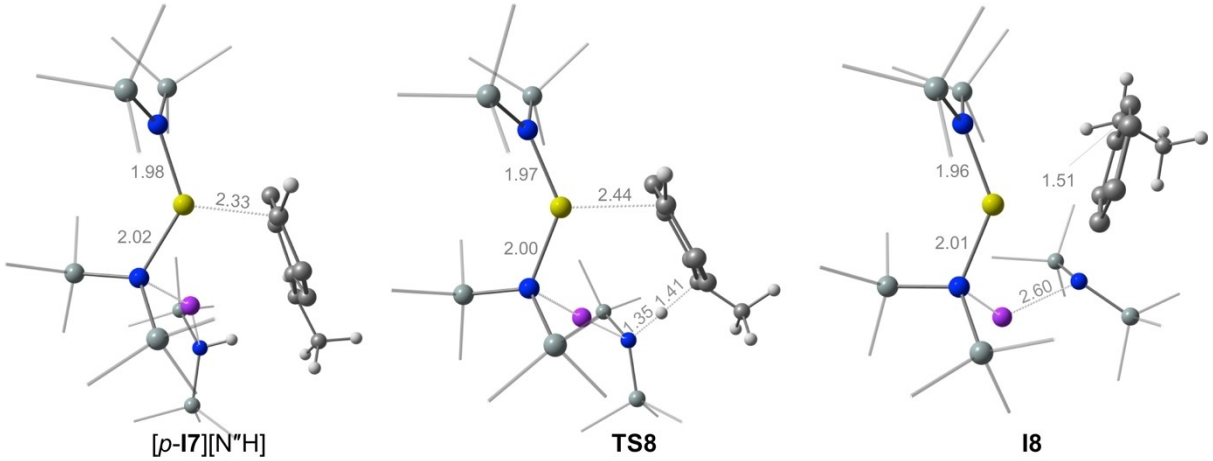

Figure 11. DFT-optimised geometries of the stationary points along the pathway for protonation of the alkyl intermediate *p*-**I7** showing key bond distances.

All compounds were structurally characterised by X-ray crystallography, revealing a common inverse crown motif of dimeric centrosymmetric $AMMg(HMDS)_2H$ units.[45,56] The structures served to authenticate the hydride complex as an intermediate in the catalytic cycle. Attempted reduction of styrene under catalytic conditions with the isolated inverse crown hydride complex $[(C_6H_6)KMg(HMDS)_2H]_2$ resulted in polymerisation of the substrate. This observation can be attributed to the absence of sufficient concentrations of N″H to enable protonation of the styryl intermediate and prevent chain growth steps. A mechanism involving the dimeric species to some degree is conceiv-

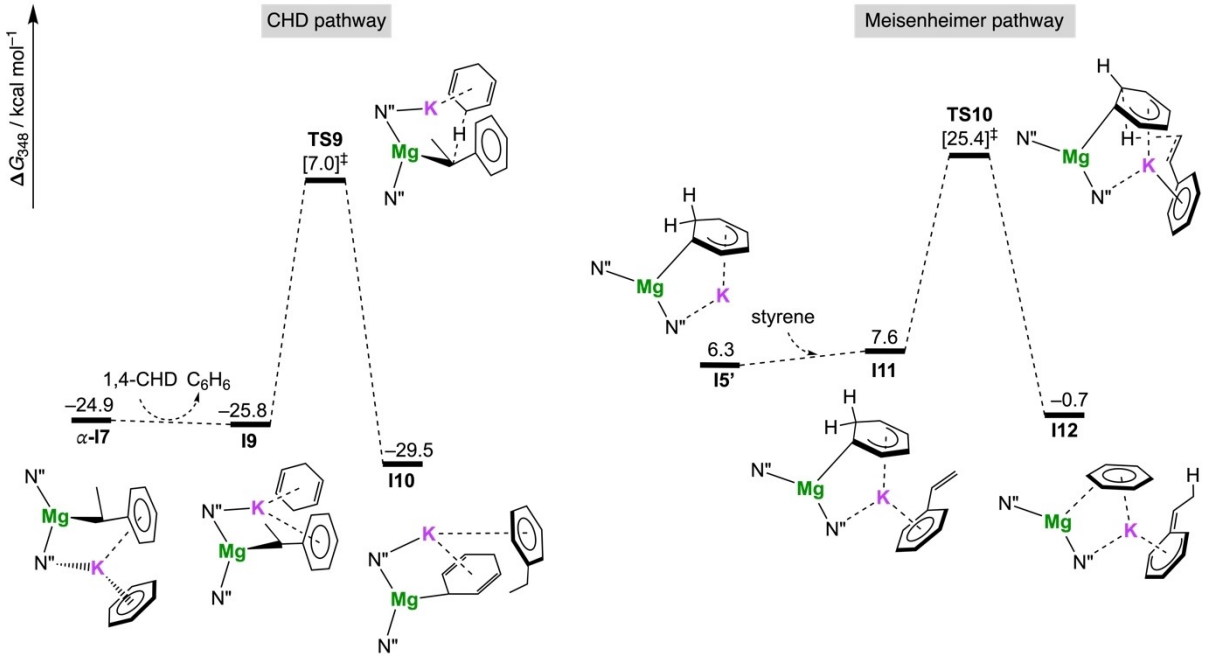

Figure 12. DFT-calculated Free Energy reaction profile (ΔG, T = 348.15 K, 1 mol L^{-1}) for two alternative pathways (CHD and Meisenheimer) in the transfer hydrogenation mediated by $(C_6H_6)K(H)MgN''_2$.

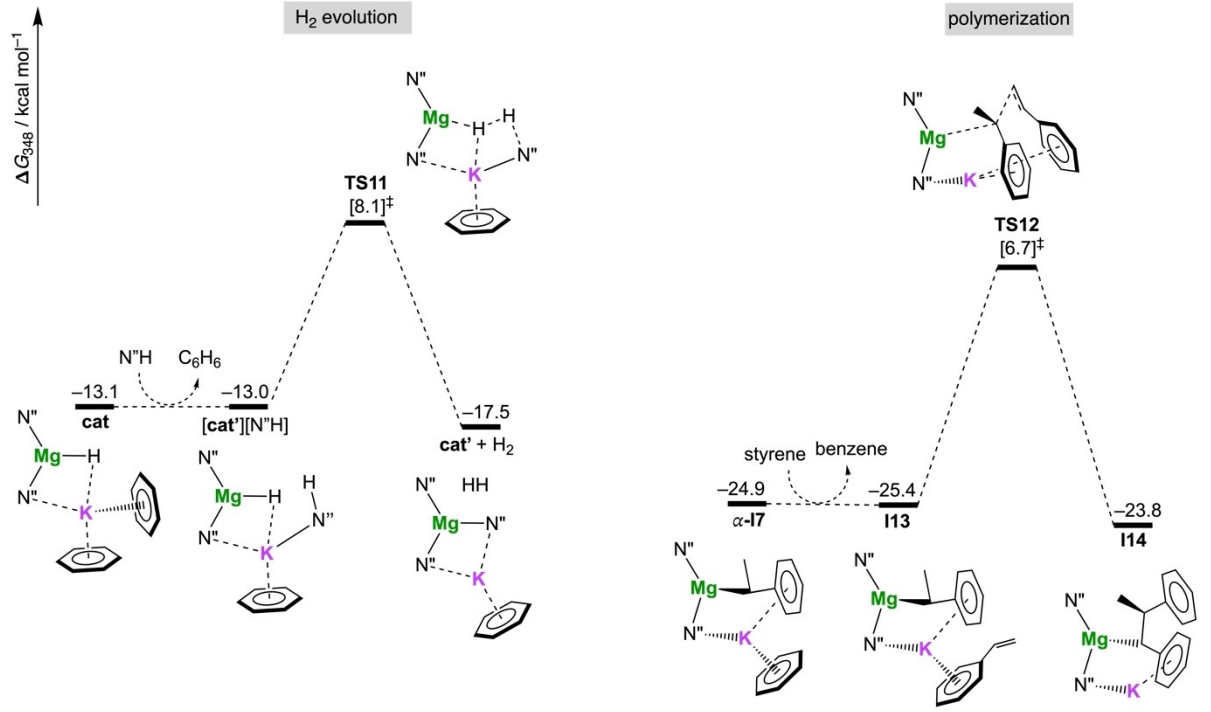

Figure 13. DFT-calculated Free Energy reaction profile (ΔG, T = 348.15 K, 1 mol L^{-1}) for two possible side reactions occurring during transfer hydrogenation mediated by $(C_6H_6)K(H)MgN''_2$.

able, provided that hydride transfer can be facilitated efficiently. We hence have studied this possibility.

The computed energy profile for transfer hydrogenation of styrene by $[(C_6H_6)KMg(HMDS)_2H]_2$ is shown in Figure 14. Formation of dimeric $[KMg(HMDS)_2H]_2$ with loss of two benzene molecules from the monomeric precursor **cat** is strongly exergonic ($\Delta G = -20.9$ kcal mol^{-1}), perhaps unsurprising given the dimeric structure of the inverse crown hydride complex.[47] The formed dimer is in equilibrium with its solvent-free counterpart, which can accept the substrate styrene through η^6-coordination to one of the potassium centres (**D-I6**, $\Delta G =$ 9.5 kcal mol^{-1}).

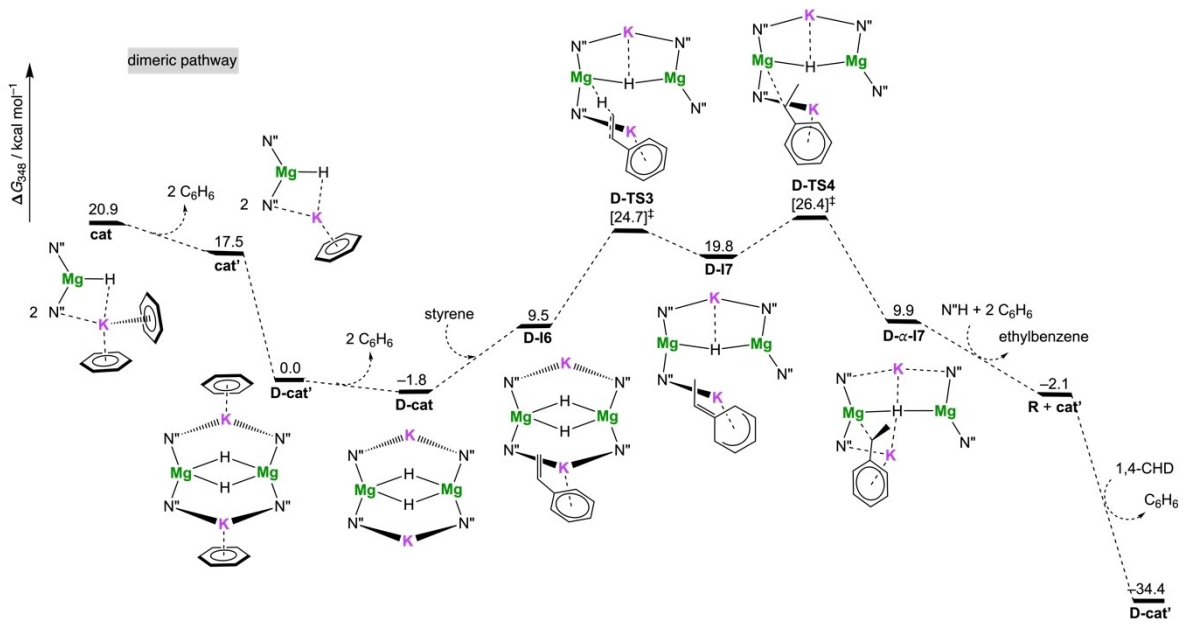

Figure 14. DFT-calculated Free Energy reaction energy profile (ΔG, T = 348.15 K, 1 mol L^{-1}) for transfer hydrogenation of styrene via dimeric $[KMg(H)N''_2]_2$.

The favourable orientation of the styrene C=C double bond with respect to the bridging hydride facilitates insertion into the terminal carbon via **D-TS3** ($\Delta G^{\ddagger}$ = 24.7 kcal mol^{-1}). Subsequent rearrangement of the unstable intermediate **D-I7**, (ΔG = 19.8 kcal mol^{-1}), which features the styrene carbanion η^6-coordinated to the K^+ centre, gives **D-*α*-I7**. (ΔG = 9.9 kcal mol^{-1} via a small barrier (**D-TS4**, 6.6 kcal mol^{-1}). From here protonation with N''H and release of ethylbenzene occurs, and the process is accompanied by slightly exergonic fragmentation of the dimeric structure into the monomeric complexes **R** and **cat'** (ΔG = −2.1 kcal mol^{-1}). It seems plausible that reformation of the dimeric magnesium hydride catalyst could occur through activation of one equivalent of 1,4-CHD by the complex **R**, followed by subsequent dimerization of two equivalents of **cat'** (ΔG = −2.1 kcal mol^{-1}). Inspection of the optimised geometry of the hydride transfer transition state **D-TS3** and the intermediates **D-I7** and **D-*α*-I7** (Figure 15) reveals that the structure undergoes a rearrangement to an open form, in which the Mg^{2+} centres are bridged by a single hydride, while the second hydride moves toward one Mg^{2+} centre where it is stabilised through secondary K···H interactions. The two Mg^{2+} ions in the fragments $[Mg(H)N''_2]$ and $[Mg(H_3CC(H)C_6H_5)N''_2]$ are separated by approximately 3.9 Å, suggesting that the structural integrity of the dimer core is lost during this transformation. The alternative (anti−)Markovnikov addition of styrene to the Mg–H–Mg bridge of the hydride dimer or the terminal Mg–H hydride unit are endergonic (7–12 kcal mol) over barriers of 33–43 kcal mol^{-1}, which are kinetically unfeasible (see Figures S10 and S11).[42] This appears to be the result of a combination of the μ_2-bridging binding mode of the hydride and steric factors, which hampers transfer onto the substrate.

Although the aggregation of the metal hydride towards a dimeric inverse crown species is thermodynamically favourable, it is difficult to obtain an estimate of the rate of formation of this dimeric species. In this context it is noteworthy that during the synthesis of $[(C_6H_6)AMMg(HMDS)_2H]_2$ (AM = Na, K) the crystalline products could only be isolated after 2–3 days at elevated temperatures, a much longer timescale compared to those of the catalytic reaction. Whilst it seems plausible that the dimeric inverse crown magnesium hydride will not form in high enough concentrations to play a significant role under catalytic conditions, we cannot rule out the dimeric pathway. Considering the initial high concentrations of the styrene and 1,4-CHD, the catalytic monomeric hydride species are formed by reaction of the $(C_6H_6)KMg(HMDS)_3$ precursor with 1,4-CHD. This hydride catalyst will be present in relatively low concentration at this stage and immediate encounters with the substrate are much more likely than self-aggregation. Nonetheless, the above mechanism provides a rationale for the experimental isolation and characterisation of $[(C_6H_6)KMg(HMDS)_2H]_2$, as well as the reactivity towards styrene polymerisation (immediate precipitation of a white solid is observed experimentally). Whilst the dimer shows some catalytic activity, reaction rates are prolonged due to its low solubility in benzene.

Conclusions

The mechanism of styrene transfer hydrogenation by the potassium magnesiate complex $KMg(HMDS)_3$ in the presence of 1,4-CHD as hydrogen source was studied in detail using DFT calculations. Its isolated component species $Mg(HMDS)_2$ and K(HMDS) (modelled as either monomer or dimer) fail to catalyse this reaction unilaterally, due to their inability to either efficiently deprotonate 1,4-CHD or selectively produce the ethylbenzene product. Combined, the bimetallic trisamide benefits from the synergistic action of its two metal centres, playing distinct but critically important roles in promoting

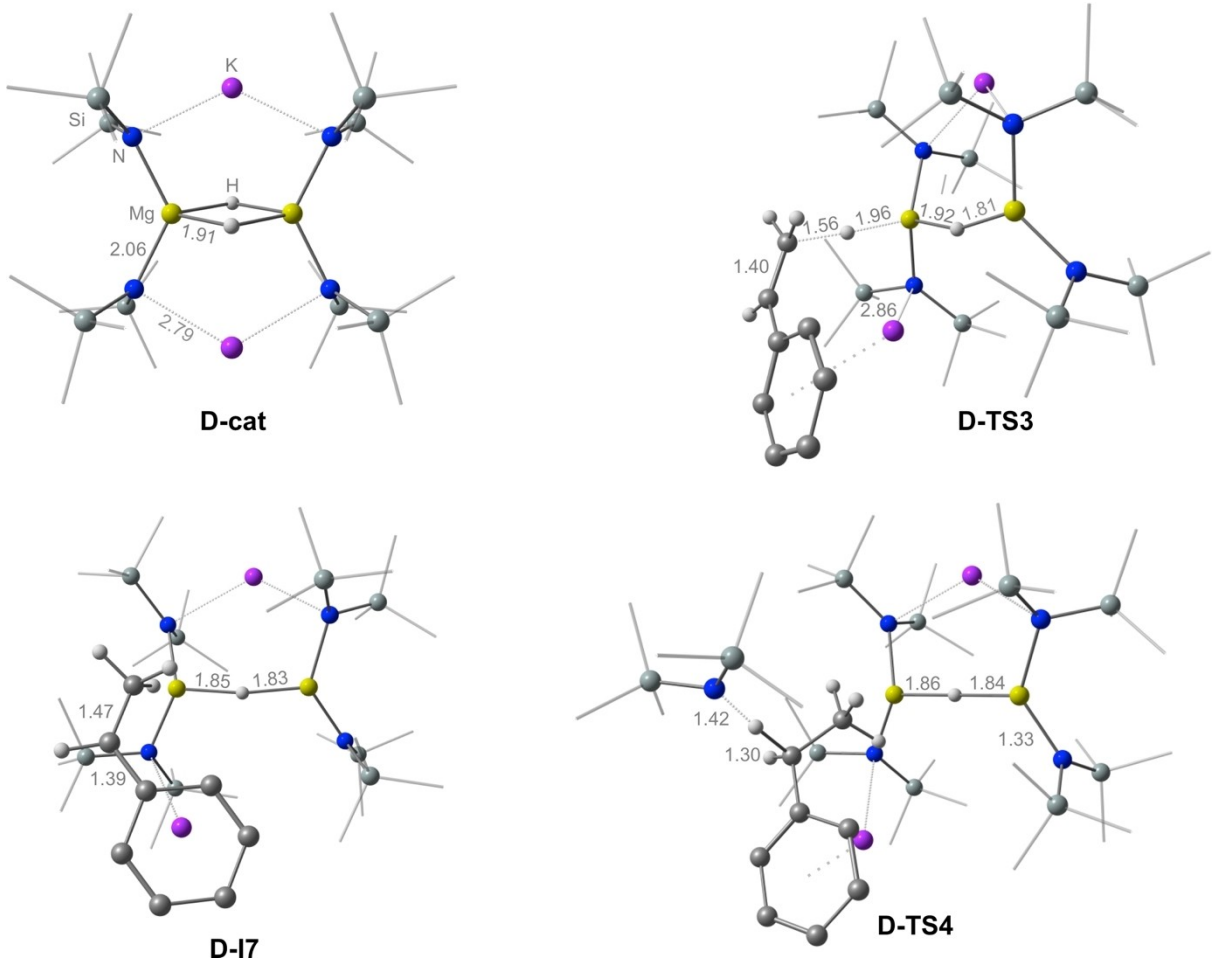

Figure 15. DFT-optimised geometries of key stationary points along the pathway for transfer hydrogenation of styrene catalysed by $[KMg(H)N''_2]_2$ showing key bond distances.

transfer hydrogenation. Generation of the catalytically active magnesiate hydride species is facilitated through an open form of $KMg(HMDS)_3$, substantially lowering the barrier to deprotonation of 1,4-CHD (**TS2**, $\Delta G^{\ddagger} = 27.9$ kcal mol^{-1}) relative to that in $Mg(HMDS)_2$ (**Mg-TS1**, 32.1 kcal mol^{-1}) or the alternative direct deprotonation (**TS2'**, 35.1 kcal mol^{-1}). Hydride abstraction by the Mg centre subsequently occurs with a moderate activation barrier (**TS3**, 19.9 kcal mol^{-1}). In the hydride transfer step to styrene (**TS4**, 10.0 kcal mol^{-1}) the potassium ion assumes the critical role of coordinating and activating the alkene substrate, again substantially lowering the activation energy in this step. Protonation of the resulting styrenyl magnesiate (**TS8**, 18.3 kcal mol^{-1}) intermediate is achieved following rearrangement of the styrene anion and stabilisation of the phenyl-centred charge by the K^+ ion. Formation of a dimeric inverse crown magnesium hydride is thermodynamically favourable. Insertion of styrene into the Mg–H–Mg bond can occur with moderate barriers (**D-TS3**, 26.5 kcal mol^{-1}), suggesting that the dimer is also catalytically competent in the hydrogenation. Recent studies have emphasised that the identity of the alkali metal can often be critical to the outcome of both stoichiometric and catalytic reactions, so one should be cautious in thinking the mechanisms favoured here for potassium would be similar to those of their lighter or heavier congeners.[22,50] Work in our group is currently ongoing to elucidate the variable facility of the alkali magnesiates in transfer hydrogenation depending on the identity of the alkali / alkaline earth metal, the substrate, as well as the solution phase speciation of the catalyst.

Computational Methods

All electronic structure calculations were performed with the Gaussian 16 (G16 revision B.01) suite of programs.[48] Full geometry optimizations of all (ground-state) species and subsequent analytical frequency calculations were carried out at the DFT level without imposing symmetry constraints. The TPSS meta-GGA exchange correlation functional was used in conjunction with the BJ-damped Grimme DFT-D3 dispersion correction,[49,50] based on the overall good performance of this meta-GGA functional in generating structures that compare well with experimental data.[42,51] A split basis set approach was utilised, to reduce computational cost during geometry optimizations. The metal centres (alkali and alkaline earth metals), atoms directly bonded to the metal centres, and atoms of small molecules relevant to key reaction steps (1,4-

cyclohexadiene, styrene and benzene) were treated with Ahlrich's def2-TZVP basis set, while the remaining atoms were treated with the def2-SV(P) basis set.[52] With this approach the bond parameters of the optimized geometry of the dimeric inverse crown complex $[(C_6H_6)KMg(HMDS)_2(H)]_2$ reproduce those of its crystallographic counterparts with very good accuracy (see Table S1). An ultrafine integration grid, corresponding to a pruned grid of 99 radial shells and 590 angular points per shell, was used for all calculations. The nature of all stationary points was identified via inspection of their analytical second derivatives. Transition states correspond to first-order saddle points on the potential energy surface with exactly one imaginary vibrational frequency corresponding to the reaction coordinate, whilst minima only contain positive vibrational frequencies. Transition states were also further confirmed by visual inspection of the imaginary vibrational mode and subsequent geometry optimisations along the displacement vector in both forward and reverse direction of the reaction coordinate, giving the nearest minima connected by a transition state. The frequency calculations also provided thermal and entropic corrections to the total free energy in gas phase at $T = 348.15$ K and $p = 1$ atm within the rigid-rotor/harmonic oscillator (RRHO) approximation.[53] Single-point calculations for accurate energies were performed using the PBE exchange correlation functional in conjunction with Ahlrich's def2-QZVP basis set, corrected for dispersion effects (D3BJ).[54,55] Gibbs Free Energies (ΔG) were corrected for benzene solvent ($\varepsilon = 2.2706$) effects using the polarisable continuum model with radii and non-electrostatic terms from Truhlar's solvation model based on density (SMD).[56] Final reaction free energies are determined from the electronic single-point energies plus TPSS-D3(BJ) thermal corrections and SMD solvation free energies, corrected for a reference concentration in solution of 1 mol L^{-1}. Of several functionals tested, the above model chemistry gave overall best agreement with the available experimental reaction times at given temperatures (see Table S2). Thermochemical data at different temperatures and concentrations were computed with the help of the GoodVibes Python program (version 3.2).[57] Visualisations of optimized geometries were created using ChemCraft (Version 1.8).[58]

Acknowledgements

The authors wish to acknowledge the Irish Centre for High-End Computing (ICHEC) for the provision of computational facilities and support. Some of the simulations were performed on the Luxembourg national supercomputer MeluXina. The authors gratefully acknowledge the LuxProvide team for their support. We thank the Irish Research Council for funding under grant number GOIPG/2022/470 (scholarship to K. M. B.). Open Access funding provided by IReL.

Conflict of Interests

The authors declare no conflicts of interest.

Data Availability Statement

The data that support the findings of this study are available in the supplementary material of this article.

Keywords: alkali metal mediation · density functional calculations · magnesiates · reaction mechanism · transfer hydrogenation

[1] J. G. de Vries, C. J. Elsevier, *The Handbook of Homogeneous Hydrogenation*, Wiley VCH, Weinheim, **2006**.
[2] S. Roseblade in *Organometallic Chemistry in Industry – A Practical Approach*, (Eds.: T. J. Colacot, C. C. C. Johansson Seechurn), Wiley VCH, **2020**, pp. 239–257.
[3] R. Noyori, *Angew. Chem. Int. Ed.* **2002**, *41*, 2008.
[4] B. J. A. Osborn, F. H. Jardine, J. F. Young, G. Wilkinson, *Chem. Commun. (London)* **1965**, 131.
[5] A. S. S. Wilson, C. Dinoi, M. S. Hill, M. F. Mahon, L. Maron, E. Richards, *Angew. Chem. Int. Ed.* **2020**, *59*, 1232.
[6] A. S. S. Wilson, C. Dinoi, M. S. Hill, M. F. Mahon, L. Maron, *Angew. Chem. Int. Ed.* **2018**, *57*, 15500.
[7] M. S. Hill, D. J. Liptrot, *Chem. Soc. Rev.* **2016**, *45*, 972.
[8] V. Leich, T. P. Spaniol, L. Maron, J. Okuda, *Angew. Chem. Int. Ed.* **2016**, *55*, 4794.
[9] D. Schuhknecht, C. Lhotzky, T. P. Spaniol, L Maron, J. Okuda, *Angew. Chem. Int. Ed.* **2017**, *56*, 12367.
[10] J. Spielmann, F. Buch, S. Harder, *Angew. Chem. Int. Ed.* **2008**, *47*, 9434.
[11] J. Spielmann, S. Harder, *Chem. Eur. J.* **2007**, *13*, 8928.
[12] H. Elsen, C. Färber, G. Ballmann, S. Harder, *Angew. Chem. Int. Ed.* **2018**, *57*, 7156.
[13] S. Harder, *Chem. Rev.* **2010**, *110*, 3852.
[14] X. Shi, G. Qin, Y. Wang, L. Zhao, Z. Liu, J. Cheng, *Angew. Chem. Int. Ed.* **2019**, *58*, 4356.
[15] X. Shi, J. Cheng, *Dalton Trans.* **2019**, *48*, 8565.
[16] H. Bauer, M. Alonso, C. Färber, H. Elsen, J. Pahl, A. Causero, G. Ballmann, F. De Proft, S. Harder, *Nat. Catal.* **2018**, *1*, 40.
[17] H. Bauer, M. Alonso, C. Fischer, B. Rösch, H. Elsen, S. Harder, *Angew. Chem. Int. Ed.* **2018**, *57*, 15177.
[18] J. Martin, C. Knüpfer, J. Eyselein, C. Färber, S. Grams, J. Langer, K. Thum, M. Wiesinger, S. Harder, *Angew. Chem. Int. Ed.* **2020**, *59*, 9102.
[19] B. De Tobel, T. A. Hamlin, C. Fonseca Guerra, S. Harder, F. De Proft, M. Alonso, *Polyhedron* **2024**, *248*, 116751.
[20] S. Das, B. De Tobel, M. Alonso, C. Corminboeuf, *Top. Catal.* **2022**, *65*, 289.
[21] H. Bauer, K. Thum, M. Alonso, C. Fischer, S. Harder, *Angew. Chem. Int. Ed.* **2019**, *58*, 4248.
[22] S. D. Robertson, M. Uzelac, R. E. Mulvey, *Chem. Rev.* **2019**, *119*, 8332.
[23] T. X. Gentner, R. E. Mulvey, *Angew. Chem. Int. Ed.* **2021**, *60*, 9247.
[24] J. M. Gil-Negrete, E. Hevia, *Chem. Sci.* **2021**, *12*, 1982.
[25] V. A. Pollard, M. Á. Fuentes, A. R. Kennedy, R. McLellan, R. E. Mulvey *Angew. Chem. Int. Ed.* **2018**, *57*, 10651.
[26] V. A. Pollard, A. Young, R. McLellan, A. R. Kennedy, T. Tuttle, R. E. Mulvey, *Angew. Chem. Int. Ed.* **2019**, *58*, 12291.
[27] L. Davin, A. Hernán-Gómez, C. McLaughlin, A. R. Kennedy, R. McLellan, E. Hevia, *Dalton Trans.* **2019**, *48*, 8122.
[28] X.-Y. Zhang, H.-Z. Du, D.-D. Zhai, B.-T. Guan, *Org. Chem. Front.* **2020**, *7*, 1991.
[29] T. X. Gentner, A. R. Kennedy, E. Hevia and R. E. Mulvey, *ChemCatChem* **2021**, *13*, 2371.
[30] H. Elsen, J. Langer, G. Ballmann, M. Wiesinger, S. Harder, *Chem. Eur. J.* **2021**, *27*, 401.
[31] A. J. Martínez-Martínez, D. R. Armstrong, B. Conway, B. J. Fleming, J. Klett, A. R. Kennedy, R. E. Mulvey, S. D. Robertson, C. T. O'Hara, *Chem. Sci.* **2014**, *5*, 771.
[32] M. G. Davidson, D. Garcia-Viva, A. R. Kennedy, R. E. Mulvey, S. D. Robertson, *Chem. Eur. J.* **2011**, *17*, 3364.
[33] S.-Y. Li, Y. Li, H.-Z. Du, J. Wu, G. Luo, B.-T. Guan, *Organometallics* **2024**, *43*, 526.
[34] A. R. Kennedy, R. E. Mulvey, R. B. Rowlings, *J. Organomet. Chem.* **2002**, *648*, 288.
[35] G. C. Forbes, A. R. Kennedy, R. E. Mulvey, B. A. Roberts, R. B. Rowlings, *Organometallics* **2002**, *21*, 5115.
[36] K. B. Starowieyski, J. Lewinski, R. Wozniak, J. Lipkowski, A. Chrost, *Organometallics* **2003**, *22*, 2458.
[37] M. Brookhart, M. L. H. Green, G. Parkin, *Proc. Nat. Acad. Sci.* **2007**, *104*, 6908.
[38] J. Klett, *Chem. Eur. J.* **2021**, *27*, 888.

[39] D. B. Pardue, S. J. Gustafson, R. A. Periana, D. H. Ess, T. R. Cundari, *Comp. Theor. Chemistry* **2013**, *1019*, 85.
[40] L. C. H. Maddock, M. Mu, A. R. Kennedy, M. García-Melchor, E. Hevia, *Angew. Chem. Int. Ed.* **2021**, *60*, 15296.
[41] W. Clegg, G. C. Forbes, A. R. Kennedy, R. E. Mulvey, S. T. Liddle, *Chem. Commun.* **2003**, 406.
[42] Z.-W. Qu, H. Zhu, R. Streubel, S. Grimme, *ACS Catal.* **2023**, *13*, 1686, and references therein.
[43] D. R. Armstrong, M. G. Davidson, D. Garcia-Vivo, A. R. Kennedy, R. E. Mulvey, S. D. Robertson, *Inorg. Chem.* **2013**, *52*, 12023.
[44] P. A. Macdonald, S. Banerjee, A. R. Kennedy, A. van Teijlingen, S. D. Robertson, T. Tuttle, R. E. Mulvey, *Angew. Chem. Int. Ed.* **2023**, *62*, e202304966.
[45] D. J. Gallagher, K. W. Henderson, A. R. Kennedy, C. T. O'Hara, R. E. Mulvey, R. B. Rowlings, *Chem. Commun.* **2002**, 376.
[46] P. C. Andrikopoulos, D. R. Armstrong, A. R. Kennedy, R. E. Mulvey, C. T. O'Hara, R. B. Rowlings, *Eur. J. Inorg. Chem.* **2003**, 3354.
[47] D. J. Liptrot, M. S. Hill, M. F. Mahon, *Chem. Eur. J.* **2014**, *20*, 9871.
[48] Gaussian 16 Revision B.01, M. J. Frisch, G. W. Trucks, H. B. Schlegel, G. E. Scuseria, M. A. Robb, J. R. Cheeseman, G. Scalmani, V. Barone, G. A. Petersson, H. Nakatsuji, X. Li, M. Caricato, A. V. Marenich, J. Bloino, B. G. Janesko, R. Gomperts, B. Mennucci, H. P. Hratchian, J. V. Ortiz, A. F. Izmaylov, J. L. Sonnenberg, D. Williams-Young, F. Ding, F. Lipparini, F. Egidi, J. Goings, B. Peng, A. Petrone, T. Henderson, D. Ranasinghe, V. G. Zakrzewski, J. Gao, N. Rega, G. Zheng, W. Liang, M. Hada, M. Ehara, K. Toyota, R. Fukuda, J. Hasegawa, M. Ishida, T. Nakajima, Y. Honda, O. Kitao, H. Nakai, T. Vreven, K. Throssell, J. A. Montgomery, Jr., J. E. Peralta, F. Ogliaro, M. J. Bearpark, J. J. Heyd, E. N. Brothers, K. N. Kudin, V. N. Staroverov, T. A. Keith, R. Kobayashi, J. Normand, K. Raghavachari, A. P. Rendell, J. C. Burant, S. S. Iyengar, J. Tomasi, M. Cossi, J. M. Millam, M. Klene, C. Adamo, R. Cammi, J. W. Ochterski, R. L. Martin, K. Morokuma, O. Farkas, J. B. Foresman, and D. J. Fox, *Gaussian, Inc.*, Wallingford CT, **2016**.
[49] J. Tao, J. P. Perdew, V. N. Staroverov, G. E. Scuseria, *Phys. Rev. Lett.* **2003**, *91*, 146401.
[50] S. Grimme, J. Antony, S. Ehrlich, H. Krieg, *J. Chem. Phys.* **2010**, *132*, 154104.
[51] B. Schirmer, S. Grimme, *Top. Curr. Chem.* **2013**, *332*, 213.
[52] F. Weigend, R. Ahlrichs, *Phys. Chem. Chem. Phys.* **2005**, *7*, 3297.
[53] S. Grimme, *Chem. Eur. J.* **2012**, *18*, 9955.
[54] M. Ernzerhof, G. E. Scuseria, *J. Chem. Phys.* **1999**, *110*, 5029.
[55] J. P. Perdew, K. Burke, M. Ernzerhof, *Phys. Rev. Lett.* **1996**, *77*, 3865.
[56] A. V. Marenich, C. J. Cramer, D. G. Truhlar, *Phys. Chem. B* **2009**, *113*, 6378.
[57] G. Luchini, J. V. Alegre-Requana, I. Funes-Ardoiz, R. S. Paton, *F1000Research* **2020**, *9*, 291.
[58] G. A. Zhurko, *Chemcraft – graphical software for visualization of quantum chemistry computations*, version 1.8 (build 654), https://www.chemcraftprog.com, Ivanovo, **2005**.

Manuscript received: April 8, 2024
Revised manuscript received: June 15, 2024
Accepted manuscript online: June 18, 2024
Version of record online: August 6, 2024